Thermoresponsive hybrid colloidal capsules as an inorganic additive for fire-resistant silicone-based coatings

Pham, Sang T, Tieu, Anh Kiet, Sencadas, Vitor, Joseph, Paul, Arun, Malavika and Cortie, David (2022) Thermoresponsive hybrid colloidal capsules as an inorganic additive for fire-resistant silicone-based coatings. Industrial and Engineering Chemistry Research, 61 (35). pp. 13104-13116. ISSN 0888-5885

I&EC research
Industrial & Engineering Chemistry Research

pubs.acs.org/IECR

Article

Thermoresponsive Hybrid Colloidal Capsules as an Inorganic Additive for Fire-Resistant Silicone-Based Coatings

Sang T. Pham,* Anh Kiet Tieu, Vitor Sencadas,* Paul Joseph, Malavika Arun, and David Cortie

Cite This: *Ind. Eng. Chem. Res.* 2022, 61, 13104−13116

Read Online

ACCESS | Metrics & More | Article Recommendations | Supporting Information

ABSTRACT: Improving the fire-resistant efficiency of silicone-based polymeric coatings is important in the building industry and electrical utilities. In this study, the water-containing hybrid calcium carbonate ($CaCO_3$)−silica (SiO_2) colloidal capsule has been developed and optimized as an inorganic flame-retardant additive. This capsule exhibits excellent thermal stability up to 1000 °C with a remaining intact hollow spherical structure. When used as an inorganic filler at 15 wt %, it not only reduces the potential fire hazards by over 44% (i.e., the sumHRC reduced from 112.00 J/g K to 62.00 J/g K) but also improves the heat-barrier efficiency by over 30% (i.e., the temperature at the steady state reduced from 350 to 360 °C to below 250 °C) of the silicone-based polymeric coatings. In addition, the capsule−polymer composite coating exhibits excellent ductility which can withstand heat-induced mechanical stresses and prevent crack propagation under radiative heating conditions. The fire-resistant mechanism of the colloidal capsule is related strongly to the encapsulated water core and the reactions between SiO_2 and $CaCO_3$ at elevated temperatures. They not only contribute to a cooling effect on the flammable pyrolysis gases but also induce the insulative effect to the resulted char during combustion. The significant advances in this study will have a high impact in customizing the functional inorganic additives for a better design of the flame-retardant composite coating.

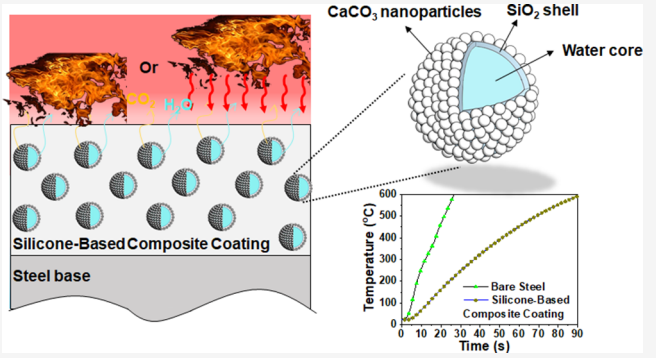

1. INTRODUCTION

Silicone-based polymers have been increasingly applied as the protective coating to protect the metallic substrates against severe environments such as humidity or dust.[1] In particular, this kind of coatings show excellent performance in corrosion protection, antifouling, anti-icing, and self-cleaning.[2] In addition, they have been recognized as a potential candidate for halogen-free flame-retardant coatings for metallic substrates.[3,4] The silicone-based polymeric coatings have superior thermal stability, low heat of combustion, a low rate of heat release, minimal sensitivity to external heat flux, and low yields of carbon monoxide release compared to conventional polymeric coatings.[5] The outstanding thermal stabilities and oxidative resistance of silicones are due to the Si−O and Si−C chemical bonds (ΔH_f = 452 kJ·mol^{-1}) which are more stable than C−C bonds (ΔH_f = 318−352 kJ·mol^{-1}).[6] Unlike traditional organic polymers, the combustion of silicones does not release any harmful/aggressive gases while producing a very small amount of smoke. In addition, silicones decompose into an inorganic silica residue that serves as an "insulating blanket." This blanket acts as a mass transport barrier reducing the volatilization of decomposition gases while insulating the underlying polymer from the incoming external heat flux.

However, the fire performance of silicone-based polymeric coatings is rather limited since they tend to crack significantly under radiative heating due to the high vibration of the Si−O bond in the infrared region prior to char development.[3] In addition, the elasticity of the siloxane chain in silicones enables the inter- and intramolecular redistribution reactions which can lead to the formation of low-molecular-weight cyclosiloxanes with lower thermal resistance compared to the theoretical calculation by considering only the chemical bonding strength.[7] This behavior induces a reduced heat-protective efficiency and the formation of noncontinuous and brittle char which is easily broken and falls off during the combustion process. Such phenomena not only deteriorate the protective capability at high temperatures but also propagate the flame which induces rapid heat transfer to the coated metallic substrate. Above 550 °C, the steel will begin to lose its structural and mechanical properties, raising safety issues such

Received: June 3, 2022
Revised: July 30, 2022
Accepted: August 12, 2022
Published: August 24, 2022

https://doi.org/10.1021/acs.iecr.2c01967
Ind. Eng. Chem. Res. 2022, 61, 13104−13116

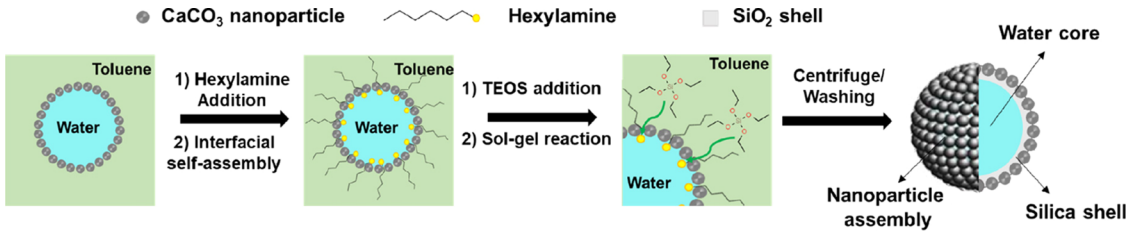

Figure 1. Schematic representing the formation of the water-containing hybrid colloidal capsules.

as the collapse of the structural building.[8] Preventing building failure due to fire to ensure a sufficient evacuation time by flame-resistant coatings[9,10] is the topmost priority for building regulations in several countries.[11]

To improve the flame resistance of the silicone-based polymeric coatings, additives are often added during the coating preparation processes. Ceramic/oxide particles, halogenated compounds, phosphorus, melamine, and their derivative compounds have been the most common flame-retardant additives used in polymeric coatings due to their good fire-retardant performance and low cost.[12−14] In particular, ceramic (oxide) inorganic fillers (i.e., silica, calcium carbonate, wollastonite, mica, etc.) can improve the flame-retardant performance by endothermic decomposition, water release, and oxide residue formation, which inhibit thermal feedback.[15,16] Meanwhile, organic-based flame-retardant additives are often chemically or physically added in the polymer matrix, which can act in the vapor phase or the solid phase to inhibit the formation of flammable gases and promote insulative char formation during combustion.[17] Currently, the use of layered materials (e.g., graphene/graphene oxides, hexagonal boron nitride, etc.) and their composites has emerged as a new class of flame-retardant additives for polymer materials.[18−20]

Microencapsulation has recently been recognized as an effective method for fire-retardant and fire-resistant innovative solutions.[21] This technique not only allows an ability to protect the sensitive compounds, e.g., organic flame retardants, but also combines several functional fillers in a single platform.[22] In addition, the synergistic effect between the materials in the microcapsule can be achieved, which significantly reduces the overall additive content in the formulation while attaining an acceptable level of fire performance.[21] The most popular feature for core−shell structures comes from the shell materials which can be adjusted for tunable permeability,[23] environmental response,[24] and external stimulus triggers.[25] Depending on the targeted application, the shell properties of the microcapsules can be finely tailored by the appropriate selection of raw materials used.

The use of ceramic silica (SiO_2) shells has shown promising performance in improving the thermal properties and water resistance of conventional flame retardants.[26−28] In addition, the SiO_2 shell has superior advantages compared to traditional polymeric shells due to its outstanding thermal, physical, and chemical stability and low permeability.[29,30] SiO_2 also has good compatibility with the silicone matrix which improves the mechanical stabilities of the coating.[31] Most recent emulsion-templated silica capsules have been synthesized with an oil core from an oil-in-water (o/w) emulsion.[32−35] However, the use of an aqueous core, water-in-oil (w/o) emulsion, is more preferable since it brings significant benefits during fire emergency while also allowing the encapsulation of several fire-retardant or fire-resistant additives, which are water soluble.[36,37] The synthesis of silica shells by the conventional sol−gel encapsulation with two emulsion systems (o/w and w/o) often produces porosity on the shell and inevitable contamination to the core materials due to the use of organic emulsifiers.[38] Additionally, the formation of aqueous-core silica capsules tends to be poorly formed compared to oil-core analogues due to the significant agglomeration and coalescence between the capsule particles.[39]

It has been found that the replacement of organic emulsifiers by the nanoparticles in the emulsification process can hinder these issues. A Pickering emulsion is formed by this approach which is distinctively stable against the coalescence and agglomeration of the emulsion droplets during the sol−gel reactions,[40] thus resulting in the formation of densely packed nanoparticles as an external layer attached to the inner SiO_2 shell, with potential to significantly improve the thermomechanical stability of the silica shell[41] while preventing the core leakage.[40]

In this study, the water-containing $CaCO_3$-decorated SiO_2 doubled-shell colloidal capsule is optimized and applied directly as an inorganic flame-retardant additive for the silicone-based polymeric coating on structural steel. The $CaCO_3$ nanoparticle is selected in this study since it is a nontoxic and environmentally friendly additive[42] that has commonly been used in the silicone industry for sealant formulation and as a fire-retardant additive.[43] In particular, the synthesis conditions were accessed and improved systematically to obtain the well-defined microcapsules. Detailed characterizations on the mechanical and thermal properties were also conducted to evaluate the robustness and thermal performance of the colloidal capsules. Further evaluation of fire performance including potential fire hazards, heat-barrier efficiency under radiative heating conditions, and the chemistry of char formation have been systematically accessed for the composite capsule-added silicone-based coating on steel.

2. EXPERIMENTAL SECTION

2.1. Colloidal Capsule Synthesis. The synthesis procedure of the colloidal capsules has been adopted from a previous study.[41] Typically, as-received stearic acid-modified $CaCO_3$ nanoparticles (50 nm), provided by the US Research Nanomaterials, were used as a stabilizing agent for the water-in-oil emulsion system. While distilled water was used as a dispersed phase, toluene (99.8%, Sigma-Aldrich) played a role as a continuous phase. The Pickering emulsion was produced under intense ultrasonication and high-shearing conditions. *n*-Hexylamine (99%, Sigma-Aldrich) and tetraethyl orthosilicate (TEOS) (98%, Sigma-Aldrich) were added to the Pickering emulsion thereafter as the catalyzing agent and the silica precursor for the hydrolysis and condensation of TEOS at the water/oil interfaces. This process resulted in the formation of a

https://doi.org/10.1021/acs.iecr.2c01967
Ind. Eng. Chem. Res. 2022, 61, 13104−13116

SiO_2 shell that enveloped the water droplets under mild stirring conditions (400 rpm). The formation of the double shell colloidal capsule is presented in Figure 1. Different synthesis conditions were conducted in this study by varying the $CaCO_3$ nanoparticle concentration (0.25, 0.5, and 1 g), the water−oil-ratio (0.25/10, 0.5/10, 1/10), the amount of TEOS (0.5, 1, and 1.5 mL), and the reaction time (12, 24, and 48 h). The resulting water-containing colloidal capsules were washed by filtration and centrifugation with acetone, ethanol, and distilled water, respectively, before drying in an oven at 40 °C for 12 h. The drying process was selected to only dry the moisture absorbed on the powder without affecting the water core.

2.2. Colloidal Capsule-Silicone-Based Polymer Composite Preparation. Different concentrations of the water-containing capsules (5, 10, 15, 20, and 25 wt %) were added to polydimethylsiloxane (PDMS, Sylgard 184), provided by Dow Inc., by a mechanical mixer operated at 3000 rpm. The yielding samples were named S184-0 wt %, S184-5 wt %, S184-10 wt %, S184−15 wt %, S184-20 wt %, and S184-25 wt %. A certain volume of the cross-linking agent was uniformly mixed to the previous blend (according to the manufacturer's instructions). The mixtures were then cast onto the surface of mild steel substrates (5 mm thick) with a thickness of 900 ± 50 μm (Figure S1a). Finally, the coatings were cured at 80 °C for a day before the fire-testing experiments. Accordingly, the density of the PDMS coatings as a function of capsule loading was measured (Figure S1b) using a pycnometer. In general, the presence of the capsules induced a decrease in the density, e.g., from 0.965 g/mL for S184-0 wt % to 0.752 g/mL for S184-15 wt %. A further increase in the capsule concentration above 15 wt % results in an increasing return of density with larger deviation. It could be due to the agglomeration of the capsules at high concentrations causing a decrease in an integrity of the composite coatings.

2.3. Mechanical Property Measurement of an Individual Capsule. The mechanical properties of the individual microcapsules were evaluated by in situ transmission electron microscopy (TEM) mechanical compression experiments (PI 95 TEM PicoIndenter holder in JEOL JEM-2010) following the approach developed by Pham et al.[41] (Figure S2). An individual colloidal capsule was compressed by a diamond tip with a circular flat-punch of D = 3 μm. The load function was set as displacement control with a constant displacement rate of 16.7 nm/s. The compression test was repeated three times in the colloidal capsules with an approximate diameter. After the experiment, the normalized strength (σ_{max}) and compressive strain (ε_f) of the colloidal capsule was calculated from the force−displacement (F−d) curve according to eqs (1) and (2):

$$\sigma_{max} = \frac{P_{max}}{\pi\left[\left(\frac{D_o}{2}\right)^2 - \left(\frac{D_i}{2}\right)^2\right]} = \frac{P_{max}}{\pi t(D_o - t)} \quad (1)$$

$$\varepsilon_f = \frac{h_f}{D_o} \quad (2)$$

where P_{max} represents the peak load and D_o, D_i, t, and h_f are the outer diameter, inner diameter, shell thickness, and compressive displacement, respectively.

2.4. Mechanical Properties of the Capsule-Added Silicone-Based Polymer Composite Coatings on Steel. The uniaxial compression test of the capsule-added silicone composite coating on steel was carried out using a universal testing machine (model 5566, from Instron) according to the ASTM D695-15 standard. A sample was placed between the compression plates with a chosen load cell of 10 kN. The samples had a round disk shape with a diameter of 10.96 mm and a total thickness (coating + steel) of 2.0 ± 0.1 mm. The load was gradually applied to the sample with a speed of 0.5 mm/min. Three independent experiments were performed for each sample and the results are presented as an average.

2.5. Fire Performance Testing of the Capsule-Added Silicone-Based Polymer Composite Coating on the Mild Steel Substrate. The composite coatings' flammability was studied by pyrolysis combustion flow calorimetry (PCFC), according to the ASTM D7309 standard.[44,45] In the present study, PCFC was chosen as a rapid screening technique as it only requires a few milligrams of a polymer for testing and often provides a wealth of combustion-related data. This technique works on a principle of oxygen depletion calorimetry relating to Huggett's principle. In the present investigation, the silicone-based composites were rapidly heated to a state of controlled pyrolysis in an inert nitrogen atmosphere (anaerobic conditions). The standard PCFC experimental protocol was modified according to Schartel et al.[45] to access the multistep decomposition of the polymer containing the fire-retardant additive. For each run, a certain amount of sample was first heated to about 900 °C at a heating rate of 1 °C/s, in a stream of nitrogen flowing at a rate of 80 cm^3/min. The volatile thermal degradation products were then mixed with a stream of pure oxygen (at a flow rate of 20 cm^3/min) before entering a combustion chamber maintained at 900 °C. All the tests were run in triplicate to ensure the reliability of the results, and the average values are reported.

A small-scale test of heat-barrier efficiency has been developed based on the previous literature[3] that produces a good correlation to the large-scale furnace test for intumescent paint-coated steel.[46] Briefly, the upper side of the sample, comprising the protective coating on the steel substrate, undergoes an external heat flux from a heat gun (Bosch PHG 630 DCE, 2000 W, 22.5 mm gun nozzle). The temperature at the backside of the sample (the steel surface) is recorded by a flexible thermocouple connected to a data logger. The coated steel samples are placed 4 cm under the heat gun, whose temperature is constantly set at 630 °C (displayed temperature). Under the setting conditions, the heat gun provides a constant hot airflow of 0.5 m^3/min, a temperature at the nozzle outlet of approximately 580 °C, and a temperature at the sample exposed surface of approximately 455 °C. Fire performance of the optimized composite coating was evaluated by the torch test method introduced by the US Bureau of Mines Fire Endurance Test (4) in 1996.[3] The coating on the steel is exposed to an open butane flame that has a maximum temperature of 1430 °C. The nozzle diameter of the butane torch was 20 mm, and the sample was held at a constant distance of 80 mm from the nozzle outlet. The temperature at the backside of the steel was recorded over time. Such design allows the tentative evaluation of the fire performance of an intumescent coating under a radiative/convective heating scenario.

2.6. Sample Characterization. Scanning electron microscopy (SEM, FEI Helios G3 CX), TEM (JEOL JEM-2010), and energy-dispersive X-ray spectroscopy (EDS) were utilized to study the structure, morphology, and composition of the

https://doi.org/10.1021/acs.iecr.2c01967
Ind. Eng. Chem. Res. 2022, 61, 13104−13116

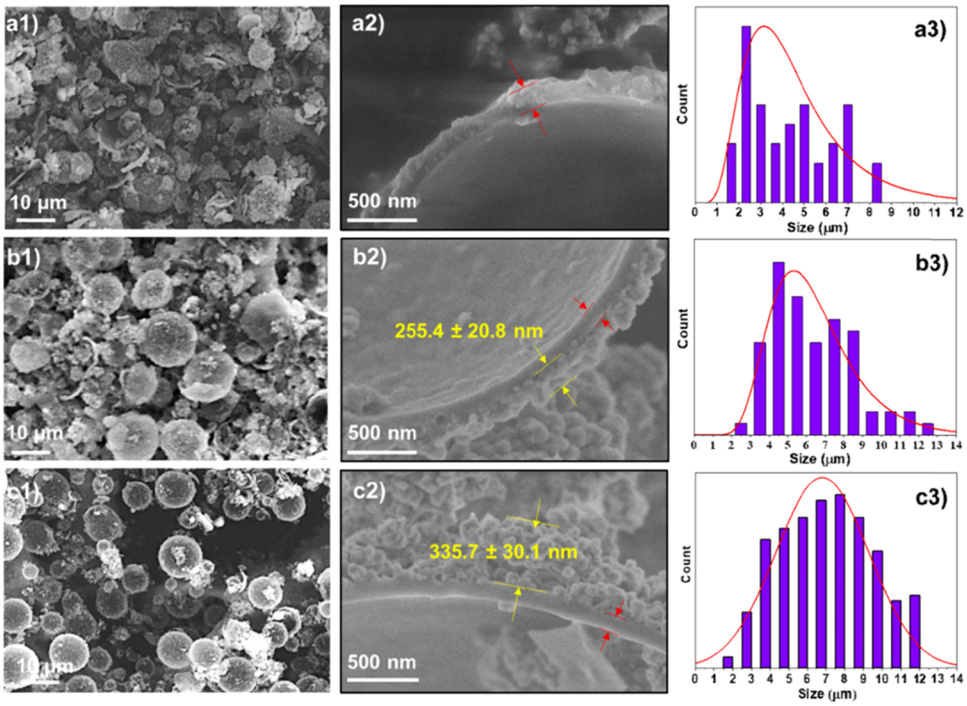

Figure 2. SEM images showing the effect of $CaCO_3$ nanoparticle amounts: (a) 0.25 g, (b) 0.5 g, and (c) 1 g on the formation of the colloidal capsules with a constant water-in-oil (w/o) ratio of 1/10 and TEOS addition of 1 mL. The overview of the capsule formation is depicted in (a1), (b1), and (c1). The observation of the shell cross-section is illustrated in (a2), (b2), and (c2). The size distribution of the obtained colloidal capsules is shown in (a3), (b3), and (c3).

samples. Thermogravimetric analysis (TGA), derivative thermogravimetry (DTG), and differential scanning calorimetry (DSC) (NETZSCH STA 449F5) were used to study the thermal behavior of the colloidal capsules from 50 to 1000 °C at a heating rate of 10 °C/min, under a nitrogen atmosphere. The in situ heating experiment was performed inside an SEM chamber (FEI Helios G3 CX) to verify the thermal robustness of the capsule. A single capsule was picked and placed on the microelectromechanical system (MEMS) chip and the in situ heating was conducted between 500 and 1000 °C with a heating rate of 5 °C/s.

The laser flash method (Linseis LFA 1000) was used to evaluate the thermal barrier of the colloidal capsules. Typically, the thermal diffusivity of the mild carbon steel and the capsule's powder-coated mild carbon steel were measured in the 30−550 °C temperature range under high-vacuum conditions. The mild carbon steel substrate used in the measurement had a diameter of 11.2 mm and a thickness of 1.2 mm. Prior to the measurement, a certain amount of colloidal capsule was coated on the steel disk by spraying using aluminum phosphate (AP) as a binder which is based on the approach from Liu et al.[47] Typically, the colloidal capsules were mechanically blended with the AP aqueous solution and the mixture was sprayed on a steel disk by compressed air spraying. Figure S3a shows that the initial thickness of the coating was 0.35 ± 0.05 mm and the surface observation of the coating shows the dense aggregation of the capsules. High-magnification observation on the coating surfaces indicates the intact spherical shape of the colloidal capsules which demonstrates the outstanding structure stability under harsh preparation conditions. Since the thickness of the coating remained approximately the same after heating at 550 °C (Figure S3b), thermal diffusivity was fitted by the combined model developed by Dusza et al.[48] All measurements were repeated at least three times to ensure their reproducibility.

3. RESULTS AND DISCUSSION

3.1. Formation Mechanism of $CaCO_3$-Decorated SiO_2 Doubled-Shell Colloidal Capsules. The colloidal capsules were fabricated using an inverse Pickering emulsion stabilized by stearic acid-coated $CaCO_3$ nanoparticles. Due to the hydrophobic nature of stearic acid, the nanoparticles were preferably deposited at the water−oil interfaces and stabilized the water-in-oil emulsion system. It has been found that the concentration of the nanoparticles in the solution, as the stabilizing agent, plays an important role in the formation of the intact colloidal capsules.[22] The effect of nanoparticle concentration and the water-in-oil (w/o) ratio on the formation of the colloidal capsules is displayed in Figure 2. As observed in Figure 2a1, almost no capsule was formed and only fractured components were obtained when 0.25 g of $CaCO_3$ nanoparticles were used (with 1/10 w/o ratio), despite a stable Pickering emulsion had been established (Figure S4a). The presence of broken shells was probably due to the generation of ethanol as a side product of the sol−gel reaction which drove phase separation between a dense silica network and a dilute micellar phase.[49] It thus detached the majority of $CaCO_3$ nanoparticles out of the interfacial areas (Figure 2a2). A further increase in the concentration of $CaCO_3$ nanoparticles led to the formation of a three-dimensional network of nanoparticles surrounding the droplets,[50] thereby reducing the droplet size distribution and promoting emulsion stabilization (Figure S4a−f). The intact spherical shape of the colloidal capsule was observed when the amount of the nanoparticles reached 0.5 g (Figure 2b1) and there was a marginal fracture in the case of 1 g of $CaCO_3$ nanoparticles (Figure 2c1). The

https://doi.org/10.1021/acs.iecr.2c01967
Ind. Eng. Chem. Res. 2022, 61, 13104−13116

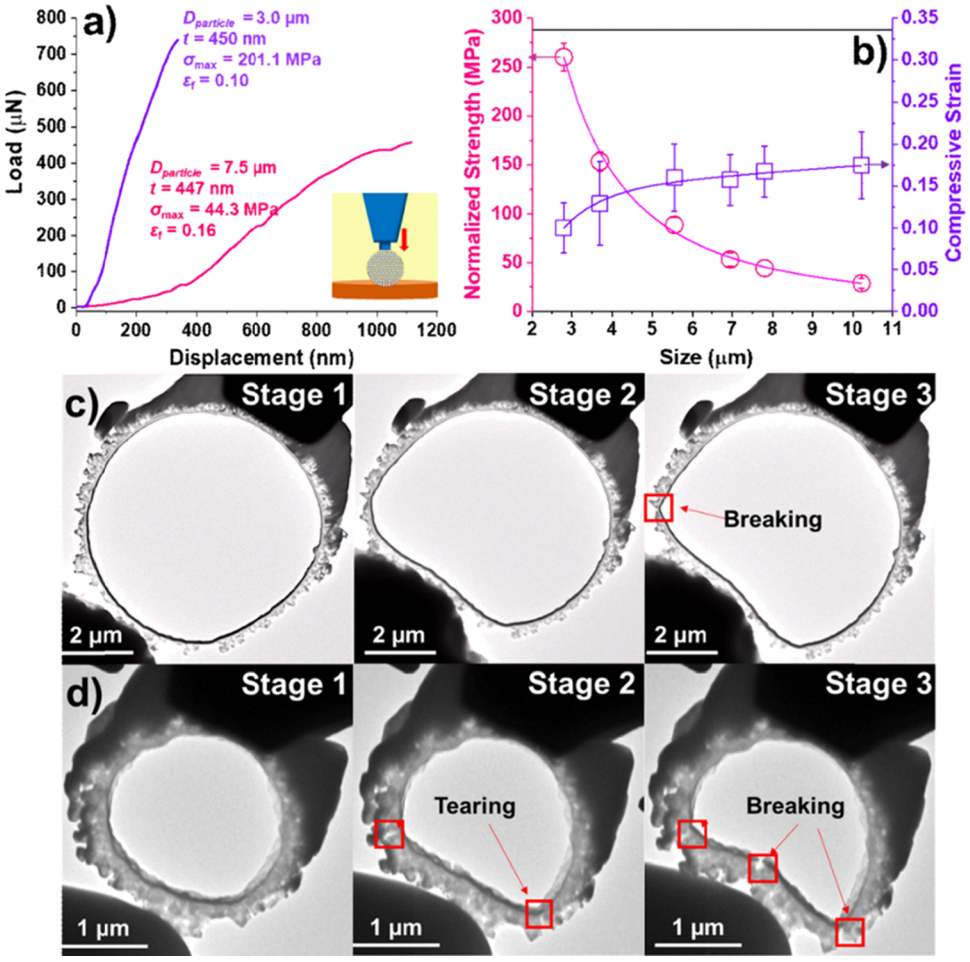

Figure 3. (a) Load−displacement curve from the mechanical compression of the 2.8 and 7.5 μm individual colloidal capsule; (b) statistic of the normalized strength and compressive strain of the colloidal capsule via the diameter. Mechanical deformation of the thin rings prepared from the large (c) and small (d) colloidal capsules.

thickness of the external shell varied from 255 ± 20 to 335 ± 30 nm with an increase in the $CaCO_3$ nanoparticles concentration in the Pickering emulsion (Figure 2b2,c2). The size distribution of the obtained colloidal capsules (Figure 2a3b3,c3) show the shift of the mean diameter toward the larger values (from 2.7 to 7.5 μm) when the amount of nanoparticles increased from 0.25 to 1 g. It is reasonable since the small emulsion droplets are encapsulated faster than the larger ones during the sol−gel reactions; thus, the smaller capsules possess sufficiently stronger shells than the larger capsules, thus being able to withstand the breakage.

Apart from the amount of nanoparticles, other synthesizing parameters, such as w/o ratio, the amount of the silica precursor (TEOS), and the reaction time of the sol−gel reactions also play a pivotal role in the formation of the intact spherical colloidal capsules. For instance, the w/o ratio shows an adverse influence on the colloidal capsule formation compared to the nanoparticle concentration (Figure S5). The lowest w/o ratio is expected to form the smaller size capsule, although they were agglomerated with the presence of the tiny nanoparticle clusters and several shell fractures (Figure S5a). It could be due to a local increase in the concentration of silicic acid in the reduced-size water droplet which led to the random collision between these molecules by Brownian movements, resulting in the nucleation of silica agglomerates that could potentially disturb the stability of the Pickering emulsion. On the other hand, the concentration of TEOS played a vital role in the formation of the intact colloidal capsule (Figure S6). The poor particle formation at low TEOS concentrations was due to the reduced silica shell thickness (98 ± 4 nm) (Figure S6a,b), which is prone to breakage during capsule collection. However, excessive TEOS amounts caused more fractures to the obtained capsules (Figure S6e,f), despite the increase in the shell thickness, probably due to the higher amount of ethanol generated during the sol−gel reaction.[49] Incomplete colloidal capsules, however, were obtained at the optimum synthesis conditions after only 12 h of sol−gel reactions, which was due to the water droplet not being fully enveloped by silica at this stage, when compared to the optimal 24 h synthesis (Figure S7a,b). However, a further increase of the reaction up to 48 h showed no changes in shell thickness (145 ± 8 nm) (Figure S7e,f) compared to the one obtained at 24 h (Figure 2c1,c2). During the shell formation, ethanol, as a side product, promoted the diffusion of water to the toluene phase.[51] It resulted in the thicker silica shell and the intact colloidal capsule over a certain time-span. When the silica shell reached a certain thickness, the shell growth rate decreased and apparently stopped as the time constant for the diffusion of water and ethanol increased significantly.

3.2. Mechanical Stability of the Colloidal Capsules.

The optimized synthesis conditions shown in Figure 2c were chosen to prepare the colloidal capsules for further evaluation

https://doi.org/10.1021/acs.iecr.2c01967
Ind. Eng. Chem. Res. 2022, 61, 13104−13116

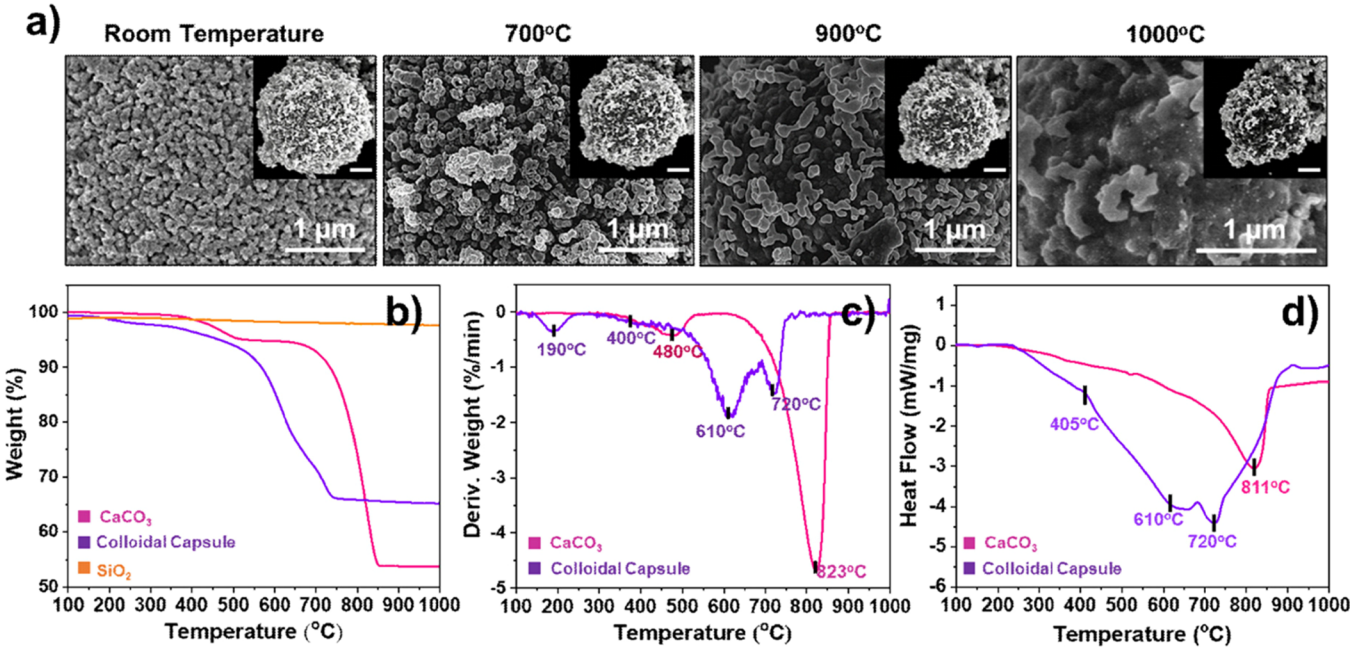

Figure 4. (a) In situ observation of the capsule's shell morphology transformation at elevated temperatures. The inset picture is the full microcapsule observation with the scale bar representing 1 μm; (b) TGA of the colloidal capsule, $CaCO_3$ nanoparticles, and SiO_2; and (c) DTG and (d) DSC of the colloidal capsule and $CaCO_3$ nanoparticles.

which resulted in a size distribution of 7.5 ± 2.4 μm (Figure 2c3). Figure 3a shows the representative load−displacement curves of the 2.8 and 7.5 μm colloidal capsules. Compared with a larger capsule (7.5 μm), the 2.8 μm tested capsule had a stiffer behavior during the mechanical compression, despite a similar brittle fracture (Figures 3a and S8). According to Figure 3b, the compressive strength rose sharply from 88.8 ± 7.9 to 260.4 ± 14.4 MPa when the capsule's diameter reduced from 5.5 to 2.8 μm, but the compressive strain decreased considerably from 0.16 ± 0.04 down to 0.09 ± 0.03. It is worth noting that the compressive strain slightly increases for all the tested capsules with a size above 5.5 μm, despite a slight decrease of the normalized strength when the particle size was increased from 5.5 to 10.2 μm. Compared to the compressive strength of the silica single-shell microcapsules, under the same diameters, from the previous study,[41] the double-shell colloidal capsules show superior compressive strength and comparable compressive strain.

The size dependence of the compressive strength and strain can be explained by observing the structure and the mechanical deformation of the thin rings prepared from the colloidal capsules with different sizes (Figure 3c,d) which shows the cross-section deformation of the shell structure. The two shells were distinct in the case of the larger ring (Figure 3c), while the smaller ring showed an ambiguous boundary between the external and internal shells (Figure 3d). In addition, the external shell of the small capsule was denser and appeared more rigid than the larger capsule. During the mechanical compression, the small ring exhibited the direct deformation of the double-shell in Stage 1 (Figure 3d), whereas the larger ring revealed the small displacement of the external shell (Stage 1, Figure 3c). The larger ring appeared ductile and flexible in the second stage and the presence of a breakage in the inner shell was observed in Stage 3 (Figure 3c). In contrast, the small ring revealed high rigidity and nonflexible performance during the deformation in Stage 2 (Figure 3d). The presence of tearing was observed before the total breakage of the whole ring (Figure 3d). Comparing the results, it can be seen that the double-shell from the small capsule behaved as a single composite shell rather than the separated hybrid-shell from the larger capsule.

3.3. Thermal Robustness and Thermal Behavior of the Colloidal Capsules. The thermal robustness of the obtained colloidal capsules is crucial for fire-retardant applications. Dynamic observation of isothermal heat-treated colloidal capsules was performed from 500 to 1000 °C under a vacuum atmosphere in an SEM chamber. According to Figure 4a and Video 1, the colloidal capsules exhibit superior thermal robustness up to 1000 °C with no distinct damages. The external shell of the colloidal capsules transformed from a granular feature to the rambutan-like structure when the temperature was increased from room temperature to 1000 °C (Figure 4a). At a temperature above 800 °C, the colloidal capsule shrunk from 5.5 to 3.1 μm, as a result of the $CaCO_3$ decomposition and a partial fusion between SiO_2 and CaO as well as the liquid sintering of the SiO_2 phase which has been demonstrated previously.[52]

TGA, DTG, and DSC were exploited to characterize the thermal behavior of the water-containing hybrid colloidal capsules (Figure 4b−d). A decrease in mass was observed from 50 to 200 °C by TGA (Figure 4b) corresponding to a mass reduction peak at 190 °C in DTG (Figure 4c) which could be due to the evaporation of the water core. A broad mass reduction peak at around 400−500 °C could be due to the decomposition of the stearic acid which was consistent with the previous study.[41] Subsequently, the decomposition of $CaCO_3$ in the colloidal capsules occurred strongly at 610 and 720 °C, respectively, that generated a noncombustible carbon dioxide gas evidenced by the significant increase in weight losses at these temperatures (Figure 4c). It has been found that $CaCO_3$ starts to degrade at around 500 °C and progresses steadily to a temperature of about 900 °C. However, the

https://doi.org/10.1021/acs.iecr.2c01967
Ind. Eng. Chem. Res. 2022, 61, 13104−13116

presence of the SiO_2 phase accelerates such decomposition processes which is due to the reactions between $CaCO_3$ and SiO_2 to produce calcium silicates and release carbon dioxide gas.[52] Since the decomposition of $CaCO_3$ is a strong endothermic process, these reactions absorbed heat from the surrounding environment (Figure 4d). The deep endothermic range of the colloidal capsule was 250−720 °C which was significantly broader than the pristine $CaCO_3$ nanoparticles (600−811 °C, Figure 4d). This result implies that the starting point to trigger heat absorption behavior was significantly decreased, which is beneficial for fire-retarded applications.

3.4. Preparation and Characterization of the Capsule-Added Silicone Composite Coating. The capsule−polymer composite was coated on the steel sample (thickness of 900 ± 50 μm, Figure S1a) as the protective barrier of the steel substrate (Figure 5a). An SEM image in Figure 5a shows the

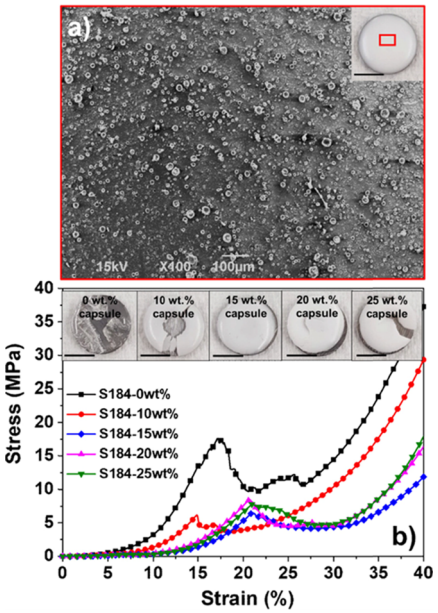

Figure 5. (a) SEM image showing the surface of the capsule-added silicone polymer coating on the steel substrate. The inset picture is the digital image showing the imaged area (red marked). (b) Stress−strain curve of the composite-coated steel samples from mechanical compression. Inset pictures showing the morphology of the coatings with different concentration of capsule additions after compression with a scale bar of 500 μm.

surface morphology of the composite coating after curing, suggesting negligible capsule agglomeration into large clusters, and demonstrates that a good dispersion of the colloidal capsules in the polymer matrix was achieved. It is expected that $CaCO_3$ nanoparticles with stearic acid-modified surfaces emerged on the surface of the densely packed external shell which improved the hydrophobicity of the colloidal capsule surface. This, in turn, enhanced their dispersibility of the capsule within the silicone polymer matrix and increased the repulsive force between the particles due to the steric effect between the long hydrocarbon chain of stearic acid.[53] In addition, the microscale spherical geometry of the colloidal capsules could prevent random aggregation compared to the nanoparticles since the resulted van der Waals attractive force at this size is negligible compared to the repulsive force.[54] Meanwhile, different heating conditions with a fan-forced heater showed almost no mass changes for the coating containing the colloidal capsules at a temperature of 20 and 40 °C whereas the coating heated at 60 °C shows a little mass reduction of 0.2 wt % after heating continuously for a month (Figure S9). It is believed that the water core inside the colloidal capsules is significantly retained under simulated hot summer condition, thus showing a promising feature for outdoor applications.

To characterize the mechanical behavior of the coating, axial compression experiments were conducted on the composite-coated steel sample. Figure S11 shows the stress−strain curve of the noncoated bare steel under compression, as a reference, which reveals an elastic deformation with a linear increase of stress via strain. Meanwhile, the shape of the stress−strain curve from the silicone-based polymeric coating resembles the behavior of the elastomer under deformation (Figure 5b). Intriguingly, an addition of the microcapsules could generally increase the ductility of the silicone-based polymer coating according to the significantly reduced stress at failure and an increase in strain at failure (Figure 5b). The significant strain before rupture (23%) was observed in the case of the S184-15 wt % sample. Such floppy and ductile characteristics improved the load-carrying ability of the capsule−polymer composite coating.

After the compression test, the S184-15 wt % composite coating was only flattened rather than crumbled (S184-0 wt %), shattered (S184-10 wt %), and cracked (S184-20 wt % and S184-25 wt %) (inset images in Figure 5b). It is anticipated that the added microcapsules, dispersed in the silicone coating with optimized concentration, could act as a stress concentrator that adsorbed the energy from mechanical compression, thus preventing crack propagation.[55] This phenomenon occurs when the capsule has a strong compatibility with the matrix and robust mechanical properties which potentially lead to crack pinning and toughening the matrix.[56] Specifically, when the composite coating experienced the loading, a fraction of the compressive energy was used to deform the capsule additives. Since the capsules had a spherical shape, the deformation of the capsules could be treated as similar to arches under a uniform loading with the stresses acting along the arch and hoop lines under compression.[57] Therefore, at the contacting point where the compressive energy impacts the capsules, the compressive behavior occurs in the nanoparticle aggregate external shell while the tensile behavior occurs in the silica inner shell. According to the Hall−Petch behavior, the nanocrystalline aggregate layer has superior yield strength due to the grain-boundary strengthening;[58] thus, the fine-grained boundaries can stop the propagation of dislocation and dissipate compressive energy and reduce plastic deformation. At high concentrations (S184-20 wt % and S184-25 wt %), the capsules tend to clump and form a cluster in the matrix which can crush each other under the compression conditions and result in numerous fracture shells within the coating matrix,[59] potentially leading to the loss of composite matrix integrity[60] and resulting in reduced ductility.

Apart from the compression test, the nanoindentation test was also performed on the virgin PDMS coating (S184-0 wt %) and composite coatings (S184-(10−25) wt %) to evaluate the wear resistance of the coatings which is important for industrial applications. The load−displacement curves for each coating are presented in Figure S10 and the nanoindentation results: hardness (H) and elastic modulus (E) are summarized in Table S1. The ratio of H/E and H^3/E^2 are used to evaluate

https://doi.org/10.1021/acs.iecr.2c01967
Ind. Eng. Chem. Res. 2022, 61, 13104−13116

Table 1. Values of Some Relevant Parameters from PCFC Runs

sample	temp to pHRR (°C)	pHRR (W/g)	THR (kJ/g)	sumHRC (J/g K)	char residue wt%
colloidal capsule	198	5.41	2.17	7.67	58.00
S184-5 wt %	604	65.10	11.40	65.00	53.10
S184-10 wt %	632	58.20	11.70	63.90	58.30
S184-15 wt %	633	57.50	11.00	62.00	60.00
S184-20 wt %	640	60.50	11.40	65.00	55.40
S184-25 wt %	637	71.90	11.30	79.70	53.20
S184-0 wt %	543	95.50	14.80	112.00	37.50

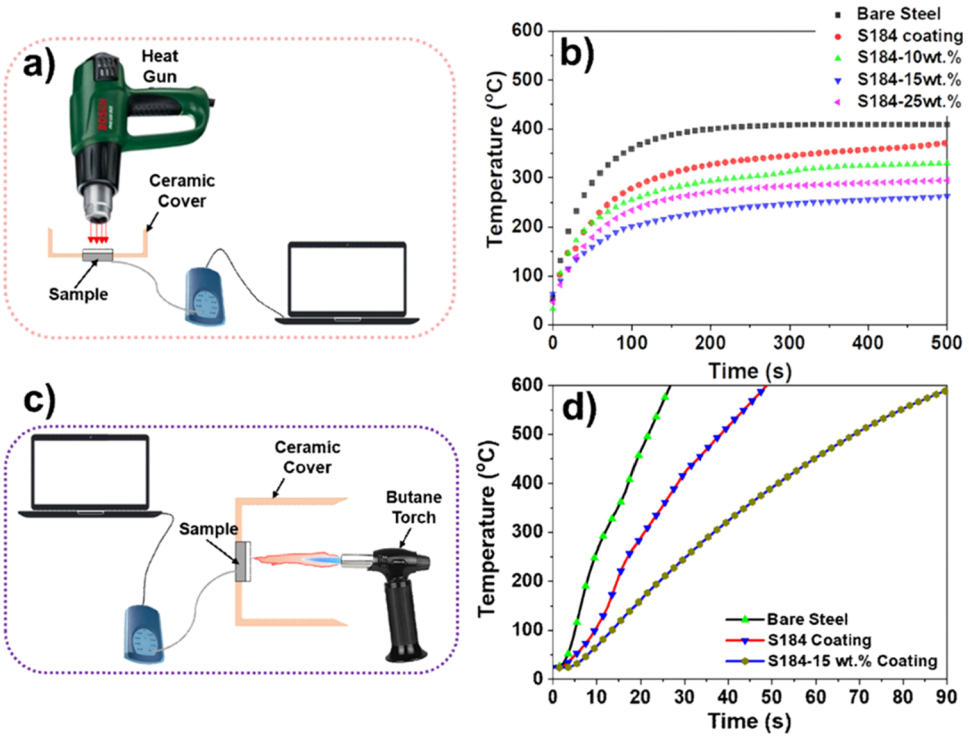

Figure 6. (a) Schematic representing the designed thermal barrier test under radiative/convective conditions; (b) time/temperature profile curves for the tested bare steel, silicone-based, and capsule-added silicone composite coatings from (a); (c) schematic representing the designed torch testing; and (d) time/temperature profile curves for the tested bare steel, silicone-based, and capsule-added silicone composite coatings from (c).

the wear resistance of the coatings according to previous study.[61] It can be seen that virgin PDMS showed $E = 1.54 \pm 0.08$ MPa and $H = 0.41 \pm 0.02$ MPa corresponding to $H/E = 0.26$ and $H^3/E^2 = 0.03$. The obtained E and H values of PDMS show consistent results to the previous study.[62] The addition of the colloidal capsules up to 15 wt % generally increased the wear resistance of the coatings, as evidenced by an increase in H/E and H^3/E^2. However, increasing the capsule loading above 15 wt % resulted in the diminishing returns of H/E and H^3/E^2 which indicates a decrease in wear resistance.

3.5. Fire Hazards of the Capsule-Added Silicone Polymer Composite. To obtain intrinsic fire hazards of the capsule-added polymer coatings with different colloidal capsule concentrations, the PCFC measurements were performed on the PDMS silicone-based polymer coatings with and without capsule addition. The following parameters were measured: the peak heat release rate (pHRR); the temperature at peak heat release rate (temperature to pHRR); total heat release (THR); sum-heat release capacity (sumHRC), and char residue amount. Although PCFC does not account for important physical effects occurring on larger scale fire testing,[45] it has been acknowledged that the obtained sumHRC (i.e., the sum of the maximum amount of heat released per unit mass per degree temperature in a multistep decomposition process) can serve as a reliable indicator for initial screening of a polymer's flammability.[44] The hybrid microcapsule exhibited the lowest values for the relevant combustion parameters including the HRC, and the char yield was one of the highest (Table 1). In contrast, the corresponding values (especially, THR and HRC) were significantly higher with the char yield being the lowest for the pure polymer (i.e., PDMS) (S184-0 wt %). This indicated a substantial degree of combustibility from the polymeric material. When the colloidal capsule was added to the PDMS polymer, the combustion parameters of the composite decreased substantially including the pHRR, THR, and HRC. In particular, the composite coatings produced substantially more char residues and this observation coupled to their relatively low values of THR and HRC can be taken as an indicative of the lower smoke production tendencies in the composite coatings, as compared to the unmodified PDMS ((S184-0 wt %). Among the composites, the sample containing 15 wt % microcapsules (S184-15 wt %) illustrated the lowest values of the mentioned parameters. In addition, this sample yielded the highest char residue which was approximately doubled compared to the pure silicone-based polymer (S184-0 wt %). It is noted that increasing the loading above 15 wt % of

https://doi.org/10.1021/acs.iecr.2c01967
Ind. Eng. Chem. Res. 2022, 61, 13104−13116

the microcapsule resulted in diminishing returns, and this effect could be exaggerated owing to the inhomogeneity in the samples that were evident through visual inspections.

3.6. Thermal Barrier Performance of the Capsule-Added Polymer Composite Coating on Steel. Thermal barrier testing was conducted to evaluate the protective efficiency of the composite coating. Figure 6a illustrates the schematic of the experimental setup. From the obtained results, it can be seen that the temperature sharply increased until it reached an almost steady state (Figure 6b). The backside of nonprotected steel established the steady state at around 410 °C after 200 s of heating. The silicone-based polymer coating (S184-0 wt %) reduced the heat transfer and resulted in the steady state at 350−360 °C. However, a moderate increase of the temperature after 450 s indicated a loss of the protective effect due to crack propagation under infrared radiation.[3] For similar tests, the capsule-added silicone-based coatings indicated a lower steady-state temperature than S184-0 wt %. The S184-15 wt % composite established the lowest steady-state temperature below 250 °C whereas S184-10 wt % and S184-25 wt % exhibited a stable temperature at 330 °C and 280 °C, respectively, after 300 s of heating (Figure 6b). Compared to S184-0 wt %, S184-15 wt % demonstrated excellent heat-barrier efficiency which reduced the steady-state temperature at the backside of the coated steel by over 30%.

The optimum S184-15 wt % coating was selected to evaluate its fire performance under a simulated fire scenario, as described in the Experimental Section. Figure 6c represents how the sample was exposed to an open flame homemade torch test. The evolution of temperature at the backside of the coated steel samples as a function of time is indicated in Figure 6d. For the nonprotected steel, the temperature rose sharply and it rapidly reached 600 °C in around 20 s. An application of S184-0 wt % coating on the steel substrate reduced the heat transfer, showing the time to reach 600 °C increased to almost 45 s. Further addition of 15 wt % colloidal capsules to the polymer-based matrix improved the heat-barrier effect significantly, and it took over 90 s to reach 600 °C, which is twice the heating time of the S184-0 wt %-coated steel.

Figure 7 reveals the surface of the composite coatings after the radiative and convective heating experiments. The presence of numerous cracks on S184-0 wt % was observable with the burning marks (Figure 7a,b). However, the cracks became reduced when 10 and 15 wt % colloidal capsules were added, but 25 wt % addition of colloidal capsules caused the reappearance of the significant cracks. At an optimum concentration (15 wt %) (S184-15 wt %), the cracks were negligible and the surface became rough and compact with the presence of nonaggregated spherical cavities (yellow arrow marked in Figure 7f). However, a large incorporation of the inorganic filler (S184-25 wt %) created a higher number of interfaces between the colloidal capsules and the polymeric matrix (Figure 7h). These particles agglomerated and were not fully covered by PDMS which lowered the integrity and led to the appearance of cracks in the coating during heat-induced mechanical stress. These cracks reduced the heat-barrier efficiency, thus increasing the temperature measured at the backside of the coated steel sample (Figure 6b, S184-25 wt %). From the obtained results, an addition of the water-containing microcapsules, at optimum concentration, can support the silicone-based polymer coating in withstanding the mechanical

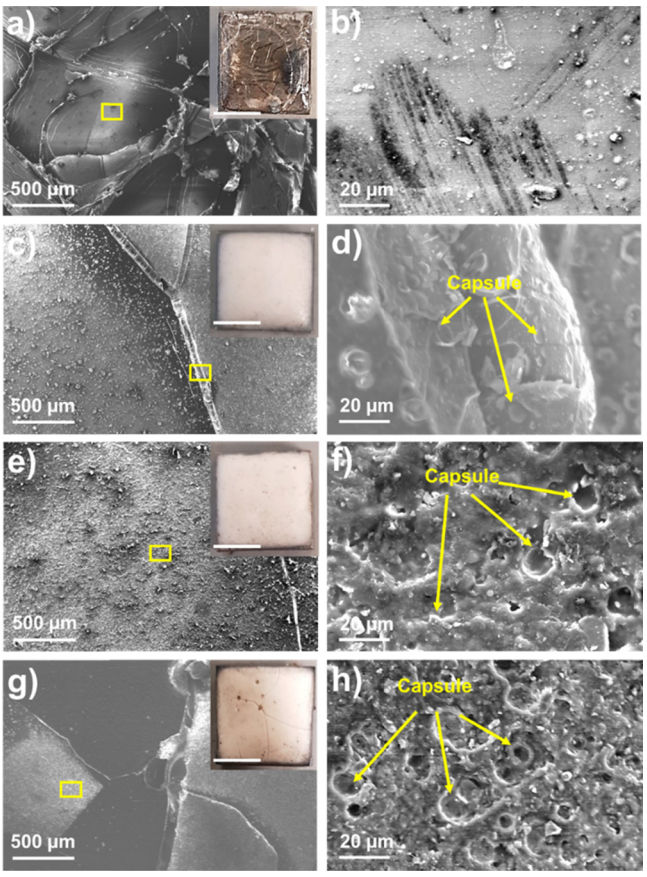

Figure 7. Surface observation after heat-radiator test of: (a,b) S184-0 wt %; (c,d) S184-10 wt %; (e,f) S184-15 wt %; and (g,h) S184-25 wt %. Inset digital images showing the overview of the samples after the heat-radiation test with a scale bar of 5 mm.

stresses induced by high temperature, thus improving the heat-barrier efficiency of the coating on steel.

3.7. Fire-Retardant Mechanism of the Composite Coatings. An investigation of the char residues after fire torch testing conditions was conducted for the S184 and S184-15 wt % samples (Figure 8). High-magnification SEM images from the char surfaces from these two samples (Figure 8a,d) show densely compact and wavy morphology composed by several sub-micrometer features fused into each other. Inset pictures in these two figures show the plane view of the coatings after combustion. While S184-0 wt % shows almost no char retaining (only the one at the edge of the steel sample—yellow arrow—inset image in Figure 8a), the S184-15 wt % coating formed rigid and compact char with significant retainment (inset image in Figure 8d). For the S184-0 wt % coating, EDS mapping analysis (Figure 8b) reveals that the char comprised mainly Si and O. XRD analysis of this char shows the distinct broad hump peak which is characteristic of amorphous materials (Figure 9a). Thus, the char residue, in this case, was completely amorphous silica (SiO_2) which is consistent with the previous literature.[63] Meanwhile, the uniform distribution of calcium (Ca) within the silica char residue was observed for the S184-15 wt % coating (Figure 8e). There is no or less intensity signal of carbon (C) from both the char residues of S184-0 wt % and S184-15 wt % indicating complete decomposition of the silicone and calcium carbonate nanoparticles. XRD analysis of the char residue from S185-15 wt % shows the distinct presence of the β-wollastonite ($CaSiO_3$) and

https://doi.org/10.1021/acs.iecr.2c01967
Ind. Eng. Chem. Res. 2022, 61, 13104−13116

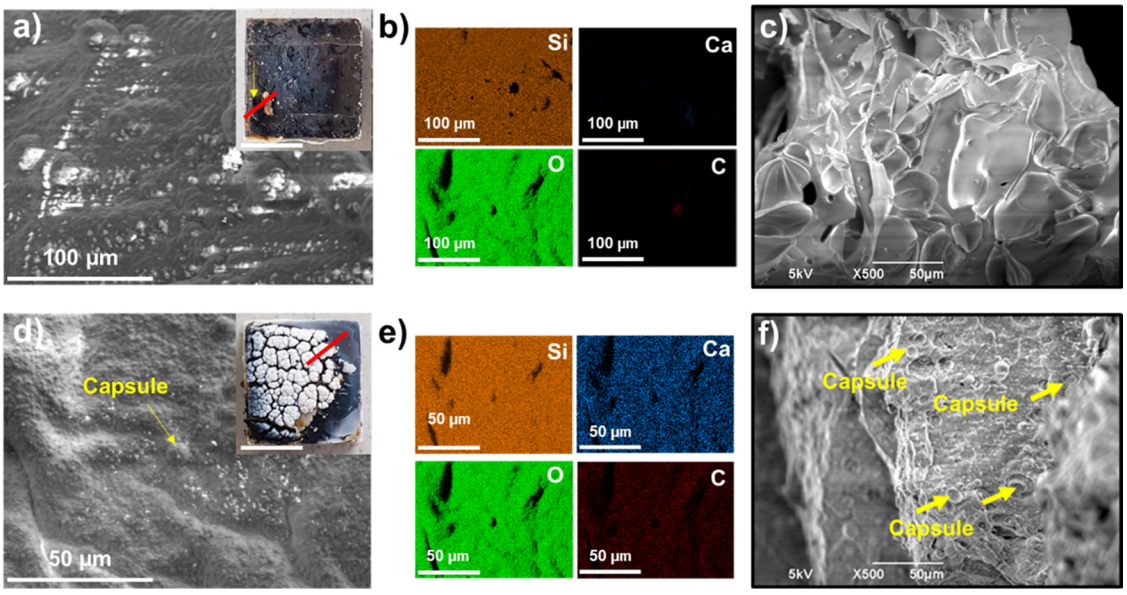

Figure 8. Plane view observation by SEM and EDS mapping analysis of the char residues after the torch test of the S184-0 wt % (a,b) and S184−15 wt % (d,e) coatings. Inset images are the digital micrograph observations of the char residues on the steel substrate after combustion tests. Internal structure observation of the char is presented in (c) for S184 and in (f) for S184-15 wt % coatings.

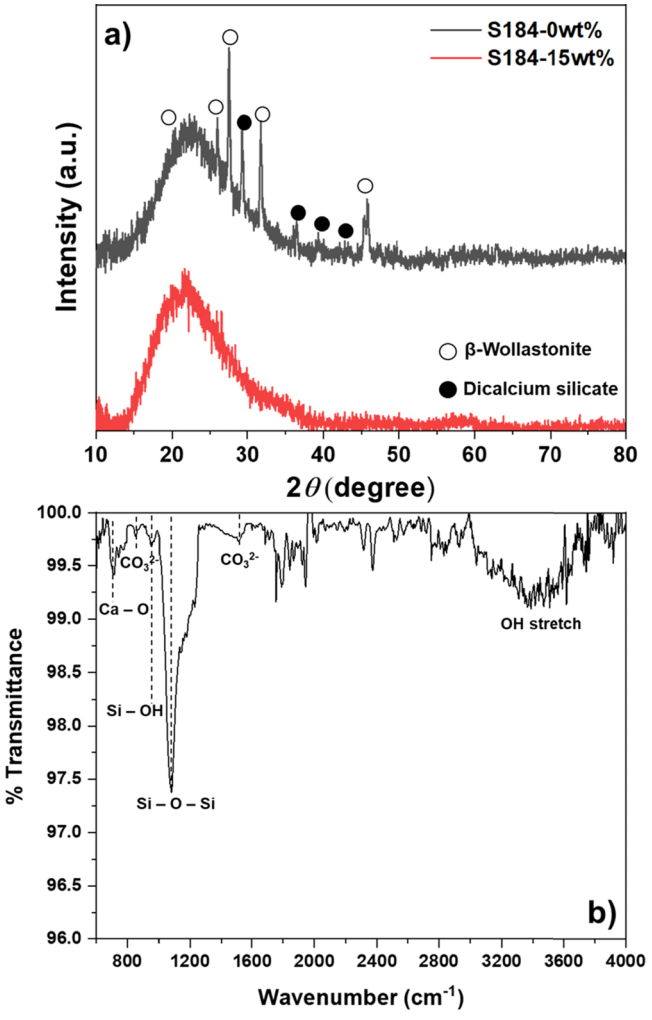

Figure 9. (a) XRD analysis of the char residues after the combustion testing of: S184-0 wt % and S184-15 wt %. (b) FT-IR analysis of the char residue after the combustion testing of S184-15 wt %.

dicalcium silicate (Ca_2SiO_4) (Figure 9) which are the common products from the reactions between $CaCO_3$ and SiO_2 at elevated temperatures.[52]

It was noted that the char formed after fire-testing conditions of S184-15 wt % was compact, rigid, and had a higher thickness than S184-0 wt % (Figure S12a,b). The thickness profile of the char was measured according to the red line in the inset pictures in Figure 8a,d. Such higher thickness was due to the evaporation of the encapsulated water and the generation of CO_2 from calcite decomposition when exposed to naked flame.[64] Further examination of the cross-section of the char (Figure 8f) shows the presence of several spherical cavities resulting from the presence of the colloidal capsules within the char (yellow arrow). Apart from the presence of the spherical cavity, a more cohesive and connected internal structure of the resulting char resides for the S184-15 wt % coating compared to the S184-0 wt % coating was observed (Figure 8f,c). An extremely porous structure with large space cavities was observed in the internal structure of the char produced from the S184-0 wt % coating (Figure 8c). The formation of large pores and space cavities has been evidenced as a characteristic of silicone (PDMS) combustion which could be the main reason for the soft, low integrity, and poor adherence of the char residues on the substrate.[65,66]

From the obtained results, the presence of the added colloidal capsules not only contributed to the formation of micrometer cavities, supplied the calcium carbonate nanoparticles, but also delivered an insulative effect to the coating. One would expect that the formation of microcavities in the char contributed to the improvement of insulation properties by increasing the traveling pathway of the conductive heat flow.[67] Such insulative effect of the colloidal capsules has been demonstrated by the thermal diffusivity measurement (Figure S13). Meanwhile, $CaCO_3$ nanoparticles had a positive effect on the thermal stability of the silicone-based polymer and additionally took an active part in the formation of the intumescent structure during fire emergencies.[15] At elevated temperatures, the water core was evaporated before the $CaCO_3$

https://doi.org/10.1021/acs.iecr.2c01967
Ind. Eng. Chem. Res. 2022, 61, 13104−13116

nanoparticles reacted to the SiO_2 shell (above 500 °C) and to the SiO_2 phase from the char to release CO_2 (Figure 4b–d). While the release of water and CO_2 under endothermic decomposition might contribute to a diluting and cooling effect on the flammable pyrolysis gases,[68] a weak base characteristic of $CaCO_3$ with the presence of water might catalyze the pyrolytic decomposition/depolymerization of a silicone matrix that favored the production of stable char and nonflammable gases.[69] Apart from such benefits, the high-temperature reactions between $CaCO_3$ and SiO_2 char caused the incorporation of calcium within the char layer (Figure 8e) that formed the calcium silicate char, as evidenced by FT-IR analysis (Figure 9b). The intense Si–O–Si band at ∼1038 cm^{-1} indicates the dominant presence of the silica phase within the char but the Ca–O band can also be recognized at ∼713 cm^{-1}. The slight detections of the CO_3^{2-} vibrations at ∼876 cm^{-1} and ∼1425 cm^{-1} indicate the retention of small amounts of calcium carbonate nanoparticles on the double-shell colloidal capsules. From the XRD analysis (Figure 9a), there is the formation of ceramic dicalcium silicate which has high ductility, high mechanical strength, and superior thermal insulation compared to amorphous silica.[70,71] Additionally, the formation of the wollastonite phase (Figure 9a) could reinforce the protective char layer leading to good mechanical properties due to the fibrous structure of wollastonite.[72] The results demonstrate a significant potential of the water-containing $CaCO_3$–SiO_2 hybrid colloidal capsules in improving the heat resistance of the silicone polymer coating.

4. CONCLUSIONS

A robust means of synthesizing the thermal-responsive water-containing colloidal capsules was conducted via Pickering emulsion-templated assembly, followed by an interfacial sol–gel reaction. It has been demonstrated that the concentration of $CaCO_3$ nanoparticles, w/o ratio, TEOS addition, and the reaction duration played a pivotal role in the successful formation of $CaCO_3$-hybridized SiO_2 doubled-shell colloidal capsules. While the concentration of $CaCO_3$ and the w/o ratio contributed significantly to the emulsion stability, the formation of the mechanically strong double shell depended mainly on TEOS addition and the reaction duration. The double-shell hybrid colloidal capsule showed excellent thermal robustness without distinctive damages at elevated temperatures (up to 1000 °C). This hybrid colloidal capsule can reduce dramatically the potential fire hazards of the PDMS polymer coating when used as an inorganic filler. The improved fire-resistant performance of silicone-based composites, as a coating on steel, has been recognized under both radiative and conductive heating scenarios. The fire-retardant mechanism was related strongly not only to the release of the water core and the thermal responsiveness of the $CaCO_3$–SiO_2 double shell but also to the thermal insulative effect of the capsule's shell and hollow structure after water evaporation. This study further introduces a novel strategy to design a microencapsulated water-based inorganic filler with desirable fire-retardant features.

■ ASSOCIATED CONTENT

Supporting Information

The Supporting Information is available free of charge at https://pubs.acs.org/doi/10.1021/acs.iecr.2c01967.

3D profile showing the capsule-added polymer coating on mild steel for the thermal barrier and fire testing, the SEM image of the prepared single colloidal capsule for in situ TEM mechanical compression, 3D profile showing the thickness of the capsule coating on mild steel for thermal diffusivity measurement, optical images of the emulsion droplets at different conditions, SEM images of the colloidal capsule formation at different synthesizing conditions, TEM images of the in situ TEM mechanical compression of the large and small colloidal capsules, the mass profile of the capsule-silicone polymer coatings via temperatures, load–displacement curves and nano-indentation results, the stress–strain curve of the steel substrate, 3D profile showing the thickness of the char obtained after the combustion of the S184-0 wt % and S184-15 wt % coatings, and thermal diffusivity measurement of the mild steel coated by the certain thickness of the capsule powder (PDF)

In situ SEM heating indicating the thermal robustness of the double shell colloidal capsule via temperature (AVI)

■ AUTHOR INFORMATION

Corresponding Authors

Sang T. Pham – *School of Mechanical, Materials, Mechatronic and Biomedical Engineering, University of Wollongong, Wollongong, NSW 2522, Australia; School of Chemical and Process Engineering, Faculty of Engineering and Physical Science, University of Leeds, Leeds LS2 9JT, U.K.;* orcid.org/0000-0002-7347-4317; Email: t.s.pham@leeds.ac.uk

Vitor Sencadas – *School of Mechanical, Materials, Mechatronic and Biomedical Engineering, University of Wollongong, Wollongong, NSW 2522, Australia; Department of Materials and Ceramic Engineering, CICECO—Aveiro Institute of Materials, University of Aveiro, 3810-193 Aveiro, Portugal*; Email: vsencadas@ua.pt

Authors

Anh Kiet Tieu – *School of Mechanical, Materials, Mechatronic and Biomedical Engineering, University of Wollongong, Wollongong, NSW 2522, Australia;* orcid.org/0000-0002-0592-8815

Paul Joseph – *Institute of Sustainable Industries and Liveable Cities, Victoria University, Melbourne, VIC 3030, Australia*

Malavika Arun – *Institute of Sustainable Industries and Liveable Cities, Victoria University, Melbourne, VIC 3030, Australia*

David Cortie – *Institute of Superconducting and Electronic Materials (ISEM), University of Wollongong, Wollongong, NSW 2522, Australia*

Complete contact information is available at: https://pubs.acs.org/10.1021/acs.iecr.2c01967

Notes

The authors declare no competing financial interest.

■ ACKNOWLEDGMENTS

The study is funded by the Australian Research Council (ARC) Discovery Project DP190103455 and Linkage Project LP160101871. The authors acknowledge the use of the JEOL 6490 SEM at the UOW Electron Microscopy Centre.

REFERENCES

(1) Wolf, A. Material properties of construction sealants. *Kautsch. Gummi, Kunstst* **1988**, *41*, 173−178.
(2) Eduok, U.; Faye, O.; Szpunar, J. Recent developments and applications of protective silicone coatings: A review of PDMS functional materials. *Prog. Org. Coat.* **2017**, *111*, 124−163.
(3) Gardelle, B.; Duquesne, S.; Rerat, V.; Bourbigot, S. Thermal degradation and fire performance of intumescent silicone-based coatings. *Polym. Adv. Technol.* **2013**, *24*, 62−69.
(4) Gardelle, B.; Duquesne, S.; Vandereecken, P.; Bourbigot, S. Characterization of the carbonization process of expandable graphite/silicone formulations in a simulated fire. *Polym. Degrad. Stab.* **2013**, *98*, 1052−1063.
(5) Barroso, G.; Li, Q.; Bordia, R. K.; Motz, G. Polymeric and ceramic silicon-based coatings—a review. *J. Mater. Chem. A* **2019**, *7*, 1936−1963.
(6) Dobkowski, Z.; Zielecka, M. Thermal Analysis of the Poly(Siloxane)−Poly(Tetrafluoroethylene) Coating System. *J. Therm. Anal. Calorim.* **2002**, *68*, 147−158.
(7) Jones, R. G.; Ando, W.; Chojnowski, J. *Silicon-containing polymers: the science and technology of their synthesis and applications*; Springer Science & Business Media, 2013.
(8) Gardner, L.; Baddoo, N. Fire testing and design of stainless steel structures. *J. Constr. Steel Res.* **2006**, *62*, 532−543.
(9) Huo, S.; Wang, C.; Hu, Q.; Liu, S.; Zhang, Q.; Liu, Z. A facile strategy to fabricate an intumescent fire-retardant coating with improved fire resistance and water tolerance for steel structure. *J. Coat. Technol. Res.* **2020**, *17*, 1401−1411.
(10) Liu, S.; Wang, C.; Hu, Q.; Huo, S.; Zhang, Q.; Liu, Z. Intumescent fire retardant coating with recycled powder from industrial effluent optimized using response surface methodology. *Prog. Org. Coat.* **2020**, *140*, No. 105494.
(11) Kobes, M.; Helsloot, I.; De Vries, B.; Post, J. G. Building safety and human behaviour in fire: A literature review. *Fire Saf. J.* **2010**, *45*, 1−11.
(12) Wilkie, C. A.; Morgan, A. B. *Fire Retardancy of Polymeric Materials*; CRC Press, 2000, p 245.
(13) Zhou, X.; Qiu, S.; Mu, X.; Zhou, M.; Cai, W.; Song, L.; Xing, W.; Hu, Y. Polyphosphazenes-based flame retardants: A review. *Composites, Part B* **2020**, *202*, No. 108397.
(14) Weil, E. D.; Choudhary, V. Flame-retarding plastics and elastomers with melamine. *J. Fire Sci.* **1995**, *13*, 104−126.
(15) Hamdani, S.; Longuet, C.; Perrin, D.; Lopez-Cuesta, J.-M.; Ganachaud, F. Flame retardancy of silicone-based materials. *Polym. Degrad. Stab.* **2009**, *94*, 465−495.
(16) Zielecka, M.; Rabajczyk, A.; Pastuszka, Ł.; Jurecki, L. Flame Resistant Silicone-Containing Coating Materials. *Coatings* **2020**, *10*, 479.
(17) Levinţa, N.; Vuluga, Z.; Teodorescu, M.; Corobea, M. C. Halogen-free flame retardants for application in thermoplastics based on condensation polymers. *SN Appl. Sci.* **2019**, *1*, 422.
(18) Zhang, Z.-H.; Chen, Z.-Y.; Tang, Y.-H.; Li, Y.-T.; Ma, D.; Zhang, G.-D.; Boukherroub, R.; Cao, C.-F.; Gong, L.-X.; Song, P.; et al. Silicone/graphene oxide co-cross-linked aerogels with wide-temperature mechanical flexibility, super-hydrophobicity and flame resistance for exceptional thermal insulation and oil/water separation. *J. Mater. Sci. Technol.* **2022**, *114*, 131−142.
(19) Guo, K.-Y.; Wu, Q.; Mao, M.; Chen, H.; Zhang, G.-D.; Zhao, L.; Gao, J.-F.; Song, P.; Tang, L.-C. Water-based hybrid coatings toward mechanically flexible, super-hydrophobic and flame-retardant polyurethane foam nanocomposites with high-efficiency and reliable fire alarm response. *Composites, Part B* **2020**, *193*, No. 108017.
(20) Huang, N.-J.; Cao, C.-F.; Li, Y.; Zhao, L.; Zhang, G.-D.; Gao, J.-F.; Guan, L.-Z.; Jiang, J.-X.; Tang, L.-C. Silane grafted graphene oxide papers for improved flame resistance and fast fire alarm response. *Composites, Part B* **2019**, *168*, 413−420.
(21) Wang, B.; Sheng, H.; Shi, Y.; Hu, W.; Hong, N.; Zeng, W.; Ge, H.; Yu, X.; Song, L.; Hu, Y. Recent advances for microencapsulation of flame retardant. *Polym. Degrad. Stab.* **2015**, *113*, 96−109.
(22) Pham, S. T.; Tieu, A. K.; Sencadas, V.; Lei, W.; Liu, D.; Wan, S.; Hao, J. Smart-Responsive Colloidal Capsules as an Emerging Tool to Design a Multifunctional Lubricant Additive. *ACS Appl. Mater. Interfaces* **2021**, *13*, 7714−7724.
(23) Kim, J.-W.; Fernández-Nieves, A.; Dan, N.; Utada, A. S.; Marquez, M.; Weitz, D. A. Colloidal assembly route for responsive colloidosomes with tunable permeability. *Nano Lett.* **2007**, *7*, 2876−2880.
(24) Johnston, A. P.; Cortez, C.; Angelatos, A. S.; Caruso, F. Layer-by-layer engineered capsules and their applications. *Curr. Opin. Colloid Interface Sci.* **2006**, *11*, 203−209.
(25) Liu, L.; Wang, W.; Ju, X.-J.; Xie, R.; Chu, L.-Y. Smart thermo-triggered squirting capsules for nanoparticle delivery. *Soft Matter* **2010**, *6*, 3759−3763.
(26) Ni, J.; Chen, L.; Zhao, K.; Hu, Y.; Song, L. Preparation of gel-silica/ammonium polyphosphate core-shell flame retardant and properties of polyurethane composites. *Polym. Adv. Technol.* **2011**, *22*, 1824−1831.
(27) Wang, B.; Tai, Q.; Nie, S.; Zhou, K.; Tang, Q.; Hu, Y.; Song, L. Electron beam irradiation cross linking of halogen-free flame-retardant ethylene vinyl acetate (EVA) copolymer by silica gel micro-encapsulated ammonium polyphosphate and char-forming agent. *Ind. Eng. Chem. Res.* **2011**, *50*, 5596−5605.
(28) Wang, B.; Hu, S.; Zhao, K.; Lu, H.; Song, L.; Hu, Y. Preparation of polyurethane microencapsulated expandable graphite, and its application in ethylene vinyl acetate copolymer containing silica-gel microencapsulated ammonium polyphosphate. *Ind. Eng. Chem. Res.* **2011**, *50*, 11476−11484.
(29) Avnir, D. Organic chemistry within ceramic matrixes: doped sol-gel materials. *Acc. Chem. Res.* **1995**, *28*, 328−334.
(30) Pagliaro, M. *Silica-based materials for advanced chemical applications*; Royal Society of Chemistry, 2009.
(31) Demir, M. M.; Menceloglu, Y. Z.; Erman, B. Effect of filler amount on thermoelastic properties of poly(dimethylsiloxane) networks. *Polymer* **2005**, *46*, 4127−4134.
(32) Yow, H. N.; Routh, A. F. Formation of liquid core−polymer shell microcapsules. *Soft Matter* **2006**, *2*, 940−949.
(33) Hayashi, K.; Nakamura, M.; Ishimura, K. In situ synthesis and photoresponsive rupture of organosilica nanocapsules. *Chem. Commun.* **2011**, *47*, 1518−1520.
(34) O'Sullivan, M.; Zhang, Z.; Vincent, B. Silica-shell/oil-core microcapsules with controlled shell thickness and their breakage stress. *Langmuir* **2009**, *25*, 7962−7966.
(35) Zoldesi, C. I.; Imhof, A. Synthesis of monodisperse colloidal spheres, capsules, and microballoons by emulsion templating. *Adv. Mater.* **2005**, *17*, 924−928.
(36) O'Sullivan, M.; Vincent, B. Aqueous dispersions of silica shell/water-core microcapsules. *J. Colloid Interface Sci.* **2010**, *343*, 31−35.
(37) Zhang, H.; Balram, A.; Tiznobaik, H.; Shin, D.; Santhanagopalan, S. Microencapsulation of molten salt in stable silica shell via a water-limited sol-gel process for high temperature thermal energy storage. *Appl. Therm. Eng.* **2018**, *136*, 268−274.
(38) Zhang, L.; D'Acunzi, M.; Kappl, M.; Auernhammer, G. K.; Vollmer, D.; van Kats, C. M.; van Blaaderen, A. Hollow silica spheres: synthesis and mechanical properties. *Langmuir* **2009**, *25*, 2711−2717.
(39) Du, X.; He, J. Spherical silica micro/nanomaterials with hierarchical structures: Synthesis and applications. *Nanoscale* **2011**, *3*, 3984−4002.
(40) Bollhorst, T.; Rezwan, K.; Maas, M. Colloidal capsules: nano- and microcapsules with colloidal particle shells. *Chem. Soc. Rev.* **2017**, *46*, 2091−2126.
(41) Pham, S. T.; Tieu, K. A.; Wan, S.; Hao, J.; Nguyen, H. H.; Mitchell, D. R. G.; Sencadas, V. Intrinsic Effect of Nanoparticles on the Mechanical Rupture of Doubled-Shell Colloidal Capsule via In Situ TEM Mechanical Testing and STEM Interfacial Analysis. *Small* **2020**, *16*, No. 2001978.
(42) DeArmitt, C.; Rothon, R. Fancy fillers. *Plast. Addit. Compd.* **2005**, *7*, 28−31.

https://doi.org/10.1021/acs.iecr.2c01967
Ind. Eng. Chem. Res. 2022, 61, 13104−13116

(43) Xu, X.; Tao, X.; Gao, C.; Zheng, Q. Studies on the steady and dynamic rheological properties of poly (dimethyl-siloxane) filled with calcium carbonate based on superposition of its relative functions. *J. Appl. Polym. Sci.* **2008**, *107*, 1590−1597.
(44) Cogen, J. M.; Lin, T. S.; Lyon, R. E. Correlations between pyrolysis combustion flow calorimetry and conventional flammability tests with halogen-free flame retardant polyolefin compounds. *Fire Mater.* **2009**, *33*, 33−50.
(45) Schartel, B.; Pawlowski, K. H.; Lyon, R. E. Pyrolysis combustion flow calorimeter: A tool to assess flame retarded PC/ABS materials? *Thermochim. Acta* **2007**, *462*, 1−14.
(46) Jimenez, M.; Duquesne, S.; Bourbigot, S. High-throughput fire testing for intumescent coatings. *Ind. Eng. Chem. Res.* **2006**, *45*, 7475−7481.
(47) Liu, M.; Hou, Y.; Li, J.; Tie, L.; Peng, Y.; Guo, Z. Inorganic adhesives for robust, self-healing, superhydrophobic surfaces. *J. Mater. Chem. A* **2017**, *5*, 19297−19305.
(48) Dusza, L. Combined solution of the simultaneous heat loss and finite pulse corrections with the laser flash method. *High Temp. - High Pressures* **1995**, *27*, 467−473.
(49) Venditti, F.; Angelico, R.; Palazzo, G.; Colafemmina, G.; Ceglie, A.; Lopez, F. Preparation of nanosize silica in reverse micelles: Ethanol produced during TEOS hydrolysis affects the microemulsion structure. *Langmuir* **2007**, *23*, 10063−10068.
(50) Abend, S.; Lagaly, G. Bentonite and double hydroxides as emulsifying agents. *Clay Miner.* **2001**, *36*, 557−570.
(51) Stöber, W.; Fink, A.; Bohn, E. Controlled growth of monodisperse silica spheres in the micron size range. *J. Colloid Interface Sci.* **1968**, *26*, 62−69.
(52) Pham, S. T.; Tieu, A. K.; Sencadas, V.; Nancarrow, M. J. B.; Peleckis, G.; Nguyen, H. H. Insight into the Mechanical Behavior of Hybrid Colloidal Capsules at Elevated Temperatures by Direct Visualization of the Interfacial Solid-State Reactions. *J. Phys. Chem. C* **2021**, *125*, 17462−17473.
(53) Rong, M.; Zhang, M.; Ruan, W. Surface modification of nanoscale fillers for improving properties of polymer nanocomposites: a review. *Mater. Sci. Technol.* **2006**, *22*, 787−796.
(54) Pailthorpe, B.; Russel, W. The retarded van der Waals interaction between spheres. *J. Colloid Interface Sci.* **1982**, *89*, 563−566.
(55) Hsueh, C. H. Effects of aspect ratios of ellipsoidal inclusions on elastic stress transfer of ceramic composites. *J. Am. Ceram. Soc.* **1989**, *72*, 344−347.
(56) Zhang, X.; Wang, P.; Sun, D.; Li, X.; An, J.; Yu, T.; Yang, E.-H.; Yang, J. Dynamic plastic deformation and failure mechanisms of individual microcapsule and its polymeric composites. *J. Mech. Phys. Solids* **2020**, *139*, No. 103933.
(57) Karnovsky, I. A. *Theory of arched structures: strength, stability, vibration*; Springer Science & Business Media, 2011.
(58) Nieh, T. G.; Wadsworth, J. Hall-petch relation in nanocrystalline solids. *Scr. Metall. Mater.* **1991**, *25*, 955−958.
(59) Qiao, Y.; Wang, X.; Zhang, X.; Xing, Z. Thermal conductivity and compressive properties of hollow glass microsphere filled epoxy−matrix composites. *J. Reinf. Plast. Compos.* **2015**, *34*, 1413−1421.
(60) Fu, S.-Y.; Feng, X.-Q.; Lauke, B.; Mai, Y.-W. Effects of particle size, particle/matrix interface adhesion and particle loading on mechanical properties of particulate−polymer composites. *Composites, Part B* **2008**, *39*, 933−961.
(61) Leyland, A.; Matthews, A. On the significance of the H/E ratio in wear control: a nanocomposite coating approach to optimised tribological behaviour. *Wear* **2000**, *246*, 1−11.
(62) Wang, Z.; Volinsky, A. A.; Gallant, N. D. Nanoindentation study of polydimethylsiloxane elastic modulus using Berkovich and flat punch tips. *J. Appl. Polym. Sci.* **2015**, *132*, 41384.
(63) Wu, Q.; Gong, L.-X.; Li, Y.; Cao, C.-F.; Tang, L.-C.; Wu, L.; Zhao, L.; Zhang, G.-D.; Li, S.-N.; Gao, J.; et al. Efficient Flame Detection and Early Warning Sensors on Combustible Materials Using Hierarchical Graphene Oxide/Silicone Coatings. *ACS Nano* **2018**, *12*, 416−424.
(64) Hull, T. R.; Witkowski, A.; Hollingbery, L. Fire retardant action of mineral fillers. *Polym. Degrad. Stab.* **2011**, *96*, 1462−1469.
(65) Cao, C.-F.; Wang, P.-H.; Zhang, J.-W.; Guo, K.-Y.; Li, Y.; Xia, Q.-Q.; Zhang, G.-D.; Zhao, L.; Chen, H.; Wang, L.; et al. One-step and green synthesis of lightweight, mechanically flexible and flame-retardant polydimethylsiloxane foam nanocomposites via surface-assembling ultralow content of graphene derivative. *Chem. Eng. J.* **2020**, *393*, No. 124724.
(66) Li, Y.-T.; Liu, W.-J.; Shen, F.-X.; Zhang, G.-D.; Gong, L.-X.; Zhao, L.; Song, P.; Gao, J.-F.; Tang, L.-C. Processing, thermal conductivity and flame retardant properties of silicone rubber filled with different geometries of thermally conductive fillers: A comparative study. *Composites, Part B* **2022**, *238*, No. 109907.
(67) Hu, F.; Wu, S.; Sun, Y. Hollow-Structured Materials for Thermal Insulation. *Adv. Mater.* **2019**, *31*, No. 1801001.
(68) Merk, V.; Chanana, M.; Keplinger, T.; Gaan, S.; Burgert, I. Hybrid wood materials with improved fire retardance by bio-inspired mineralisation on the nano- and submicron level. *Green Chem.* **2015**, *17*, 1423−1428.
(69) Di Blasi, C.; Galgano, A.; Branca, C. Influences of the Chemical State of Alkaline Compounds and the Nature of Alkali Metal on Wood Pyrolysis. *Ind. Eng. Chem. Res.* **2009**, *48*, 3359−3369.
(70) Vaills, Y.; Qu, T.; Micoulaut, M.; Chaimbault, F.; Boolchand, P. Direct evidence of rigidity loss and self-organization in silicate glasses. *J. Phys.: Condens. Matter* **2005**, *17*, 4889.
(71) Kilinc, E.; Hand, R. J. Mechanical properties of soda−lime−silica glasses with varying alkaline earth contents. *J. Non-Cryst. Solids* **2015**, *429*, 190−197.
(72) Hermansson, A.; Hjertberg, T.; Sultan, B.-Å. The flame retardant mechanism of polyolefins modified with chalk and silicone elastomer. *Fire Mater.* **2003**, *27*, 51−70.

https://doi.org/10.1021/acs.iecr.2c01967
Ind. Eng. Chem. Res. 2022, 61, 13104−13116